Finite Element Explicit Dynamics Simulation of an Impact Cutting Mechanism Analysis of *Populus tomentosa* Branches

Shihong Ba,[a,b] Yichen Ban,[a,b] Kun Lyu,[a,b] Yang Liu,[a,b] Jian Wen,[a,b,*] and Wenbin Li [a,b]

The branch impact failure mechanism has gradually received attention from scholars, along with the application of impact cutting methods in plantation forest pruning. In this paper, the impact cutting failure mechanism of *Populus tomentosa* branches was mainly studied. The impact cutting process of branches was simulated by using Finite Element Method (FEM)-based explicit dynamics. The stress change and deformation characteristics in the branch failure process were studied. A theoretical model of branch impact cutting mechanism with branch diameter, cutting clearance, and branch angle as the main factors was proposed. The model describes the branch cutting damage process and the changing characteristics of cutting force. A branch failure state equation was proposed to describe the branch impact cutting failure patterns. The forest experiment was conducted to validate the branch impact cutting mechanism and the branch failure state equation. This work fills a vacancy of relevant theory and provides a theoretical basis for the future development of forestry and agricultural equipment using impact cutting.

DOI: 10.15376/biores.19.2.3614-3636

Keywords: Cutting mechanics; Explicit dynamics; Finite element method; Impact pruning; Populus tomentosa

Contact information: a: College of Engineering, Beijing Forestry University, Beijing 100083, China; b: Key Laboratory of State Forestry Administration on Forestry Equipment and Automation, No.35 Tsinghua East Road, Haidian District, Beijing 100083, China;
** Corresponding author: wenjian@bjfu.edu.cn*

INTRODUCTION

Given the prospects of drastic global climate change and continuous ecological degradation, plantation forests are playing an increasing role in regulating climate, conserving soil and water, and maintaining atmospheric carbon, oxygen, and energy balance (Hartley *et al*. 2002; FAO 2016a; Zeng *et al*. 2021). *Populus tomentosa* is one of the most important fast-growing and high-yielding species in the world's mid-latitudes and is of great significance to China's ecological environment construction (FAO 2016b; Xi and Clothier 2021). *Populus tomentosa* grows rapidly and responds strongly to external factors. Therefore, maintaining and improving the productivity of *Populus tomentosa* plantation forests requires more frequent interventions than plantations of slow-growing species (Fu *et al*. 2022). Currently, due to the low average productivity of poplar plantation forests in China, China must innovate intensive poplar cultivation techniques, including pruning and nurturing. However, traditional forestry practices rely on manual work, which inevitably involves ergonomic hazards and musculoskeletal injuries (Gowda *et al*. 2011).

The introduction of mechanized forestry equipment has been highly successful in improving the productivity and safety of plantation forests (Wang *et al*. 2016).

In recent years, as industrialization has accelerated, many mechanical devices for agriculture and forestry have been successfully developed. Many scholars and companies have chosen impact operation method that utilize the inertia of the high-speed movement of the machinery to complete the operation to improve the efficiency of the operation (Mathanker *et al*. 2016; Jordan 2019; Ni *et al*. 2021; Ban *et al*. 2022; Song *et al*. 2022). Therefore, impact cutting may be the key to solving the problem of pruning in plantation forests of plantation forests in the future. However, the theoretical study on the mechanism of impact cutting is still unclear.

Understanding the deformation behavior of plant stalks under machine action is crucial in process optimization and efficiency optimization (Leblicq *et al*. 2015). However, it is currently difficult to apply standardized methods for testing the mechanical properties of plant stalks due to differences in plant species and growing environments (Shah *et al*. 2017). Currently, in addition to physical experiments, simulation techniques based on finite element methods are widely used by researchers in forestry (Davim 2011; Meng *et al*. 2019; Yang *et al*. 2021; Niu *et al*. 2022). The above research mainly focused on the cutting force response and damage of crops under the condition of low cutting speed and low strain rate. In addition, the current research has not proposed a theoretical model to describe the failure process of plant stems in detail. Impact cutting has the characteristics of transient, velocity-dependent, and large strain rate phenomena. The current research cannot be applied to the pruning equipment development based on the impact cutting principle. Considering the rapid development of related equipment, the research on impact cutting mechanism of plant stems is more urgent.

The explicit dynamics method is a time-integral based solution, which is often used in the simulation analysis of dynamic processes affected by velocity, such as free fall, impact, and collision. Obviously, impact cutting processes can be considered the domain of explicit dynamic methods. The finite element explicit dynamic simulation can obtain the dynamic behavior and stress distribution characteristics under the dynamic action of the target (ANSYS 2016). The stress parameters and deformation images obtained from the simulation results can be used to construct a theoretical model describing the crop failure process, supplementing the lack of current relevant theories. Therefore, the finite element explicit dynamic method may provide a new way for the research and development of forestry equipment.

Celik (2017a) used the explicit dynamics approach to investigate the damage susceptibility and the realistic representation of nonlinear deformation behavior over time of Ankara pears under various impact scenarios. Predictive models that can describe the magnitude of damage susceptibility of fruits for various impact scenarios on a specific impact platform were obtained (Celik 2017a). It is necessary to make appropriate assumptions about the three-dimensional model of the research target to shorten the calculation time. Zhou *et al.* (2022) studied the effect of strong seismic action on the shedding behavior of jujube fruits. The three-dimensional model of jujube fruits is determined as a centrosymmetric model, and the center of gravity of the jujube model is shifted by adjusting the density of fruits in a way that the center of gravity is shifted under the circumstance of maintaining a constant weight of the jujube model so that the jujube fruit is simulated to be more realistic (Zhou *et al*. 2022). In the process of finite element modeling, the definition of the material constitutive model of the research target is an important step in determining the correctness of the simulation results. The process of

defining the material constitutive model is a general approach to making reasonable assumptions based on the realistic structure of the research target. By observing the microstructure of pecan, Celik (2017b) has assumed elastic-perfectly brittle and elastic-plastic bilinear isotropic strain hardening assumption idealizations for pecan shell, packing material, and kernel respectively. As different plants grow in different ways, different loading conditions can greatly affect the stress-strain relationship curve of the target material. In the study of corn impact damage, Guan *et al*. (2023) conducted static compression tests on fresh corn with and without ears to determine whether the ear leaves would affect the impact damage condition of corn. In general, when using the finite element method to solve engineering problems, establishing appropriate three-dimensional models, choosing the correct principal model, and considering plant growth factors are necessary to ensure correct solution results.

The main objective of this study was to investigate the cutting mechanism of plant stems under impact operation in the case of *Populus tomentosa*, and a stress behavior-based branch failure model is proposed. The deformation behavior and stress progression of *Populus tomentosa* branches under impact cutting, especially the branch failure form, were simulated by finite element method-based explicit dynamics simulations. For this purpose, the branch failure process was investigated through three-dimensional modeling, physical testing, and finite element method-based explicit dynamics simulation, and an equation of state describing the branch failure mode is proposed. The accuracy of the finite element model and branch failure equation of state was also verified experimentally. The impact branch failure model proposed in this paper can provide a theoretical reference for the failure progression of plant stalks. The introduction of finite element explicit dynamic method provides a new way to study the large load and deformation problems in the forestry field. It can also provide a principal reference for the development of equipment based on plant stalk operation.

EXPERIMENTAL

Structure and Working Principle of Impact Pruner

The structure of the impact climbing pruning equipment is shown in Fig. 1 (Ban *et al*. 2022). It is driven by a hydraulic motor (Danfoss, Denmark) to provide climbing power. The clamping arm is powered by a cylinder (Sintered Metal Company, Japan) to fix the pruner to the tree trunk. The cutting mechanism consists of five cutters to complete the branch cutting operation. The work is divided into two phases: the climbing and pruning phase and the braking and falling phase.

In the climbing pruning stage, the pruner is powered by the hydraulic motor to climb upwards and gain cutting speed. The speed gained by the pruner climbing and the inertia of the body is utilized to complete the branch cutting operation. After completing the pruning, the hydraulic motor decelerates and brakes. The pruner slowly descends to the ground.

The operator sends commands to control the power output of the hydraulic motor through the command handle to achieve remote control. The high efficiency of the impact pruner makes it replace the manual operation to complete the large plantation pruning task. At the same time, the remote operation keeps the operator away from the damage caused by the fall of branches or debris.

The impact pruner uses the inertial force of rapid climbing to achieve pruning. The cutting process is characterized by a large strain rate, transient state, and velocity dependence. Its performance depends on its speed and inertia effects. Its theoretical model has the characteristics of collision and impact physics models. Therefore, the working mode of the pruning machine is named impact cutting.

Fig. 1. The impact pruner

Cutting Mechanism and Failure Equation

In the forest experiment, the branch failure types were divided into three patterns: impact failure, cutting failure, and laceration failure, as shown in Fig 2. Impact failure means that when the cutter contacts the branch, the cutting force F is generated, and $\boldsymbol{F}$ generates a bending moment $\boldsymbol{M}$ at the root of the branch. The branch breaks under the action of the bending moment $\boldsymbol{M}$ at the root. According to the large amount of data collected from observation, it is found that the impact failure occurs at the moment when the cutter touches the branch, and the cutter does not cut into the interior of the branch. When the laceration failure occurs, not only does the branch root damage tend to be more serious, but the branch pruning is not sufficient, which needs more pruning operation, greatly reducing the pruning efficiency. Cutting failure refers to the role of the cutting force F. The cutter cuts into the interior of the branch to cut off the branch. In this type of failure, the branch fracture cross-section is smoother, and the overall damage to the branch is smaller. During the forest experiment, there was another branch failure mode - laceration failure. In this case, the branch will be loaded by the combined bending moment $\boldsymbol{M}$ and cutting force $\boldsymbol{F}$ to produce damaged cracks in the form of tearing. The crack will continue to expand until the branch fails by fracture. The branch wound damage is extremely severe since the branch breakage is the result of many cracks. Slow wound healing tends to produce diseases such as insect or fungal damage (Maurin and Rochers 2013). Clearly, cutting failure is a branch failure mode that meets the design expectations of forestry equipment due to the low level of branch damage produced. However, there is no complete theory describing the mechanism of branch failure. Therefore, it is important to explore how all failures are generated for the subsequent optimization of pruners.

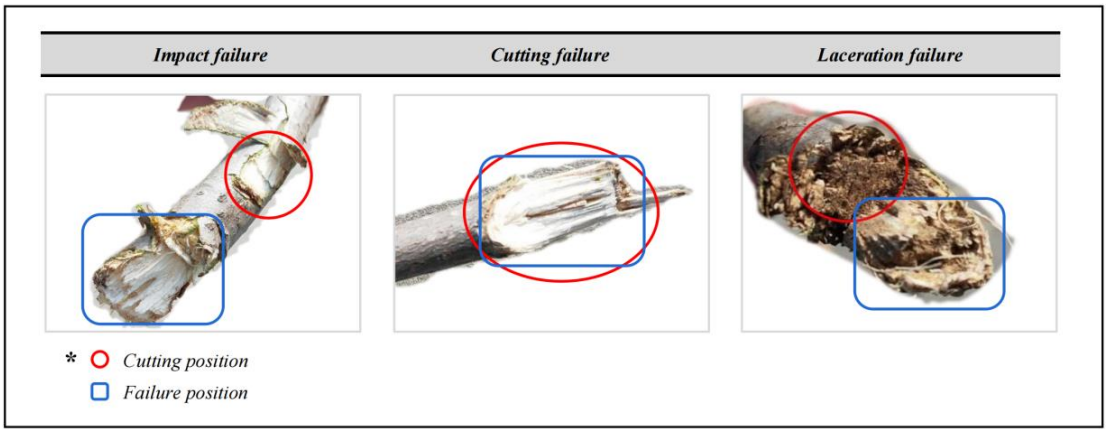

Fig. 2. Failure patterns

Because the strength and hardness of the cutter are much higher than the branch, it is assumed that the cutter is a rigid body and the branch is an elastic body with an elastic coefficient of ***k***, as shown in Fig. 3-(1). In this analytical model, the branch can be thought of as a linear dynamic system whose load is the inertial force of a pruner moving upward in the direction of the trunk. In this case, the branch can be regarded as a Single-Degree-Of-Freedom (SDOF) cantilever beam. The equations of motion control are as follows.

$$\boldsymbol{m\ddot{x}(t) + c\dot{x}(t) + kx(t) = 0} \quad (1)$$

where ***m*** is the mass of the branch(kg), ***c*** is the damping of the branch and ***k*** is the elastic coefficient of the branch. In the case of undamped systems, ***c*** becomes zero, forming Eq. 2.

$$\boldsymbol{m\ddot{x}(t) + kx(t) = 0} \quad (2)$$

In the above analysis, ***F*(*t*)** represents the dynamic force applied to the branch due to the impact pruner (N), which is a half-sinusoidal pulse of pulse duration *T*(s), which should be equal to:

$$\boldsymbol{F(t) = \begin{cases} F_{max}\sin(\pi\frac{t}{T}), & t < T \\ 0, & t \geq T \end{cases}} \quad (3)$$

Because the branch is treated as an elastomer, the following relationship is obtained.

$$\boldsymbol{x = \frac{v}{\omega}sin\omega t} \quad (4)$$

$$\boldsymbol{\omega = \sqrt{\frac{k}{m}}} \quad (5)$$

$$\boldsymbol{F(t) = kx = v\sqrt{km}sin(\sqrt{\frac{k}{m}}t)} \quad (6)$$

$$\boldsymbol{T = \frac{\pi}{\omega} = \pi\sqrt{\frac{m}{k}}} \quad (7)$$

$$\boldsymbol{F_{max} = F(\frac{T}{2}) = v\sqrt{km}} \quad (8)$$

where ***x*** is the deformation quantity of branch (m), ***ω*** is the angular frequency (rad/s), and ***v*** is the cutting speed (m/s).

In this system, it is obvious that the force *F* generated when the branch comes into contact with the cutter is proportional to the cutting speed *v*, to the $\sqrt{m}$, and to the $\sqrt{k}$. It means that the greater the pruner mass or the cutting speed *v*, the higher the cutting force *F* will be. The higher the mass of the pruner or the higher the cutting speed *v*, the higher the cutting force *F* during pruning. However, it should be noted that the above model cannot describe the material damage that occurs after a collision. Nevertheless, it is possible to apply the above theory to the instantaneous moment of the collision and make a theoretical estimation of the magnitude of the cutting force *F*.

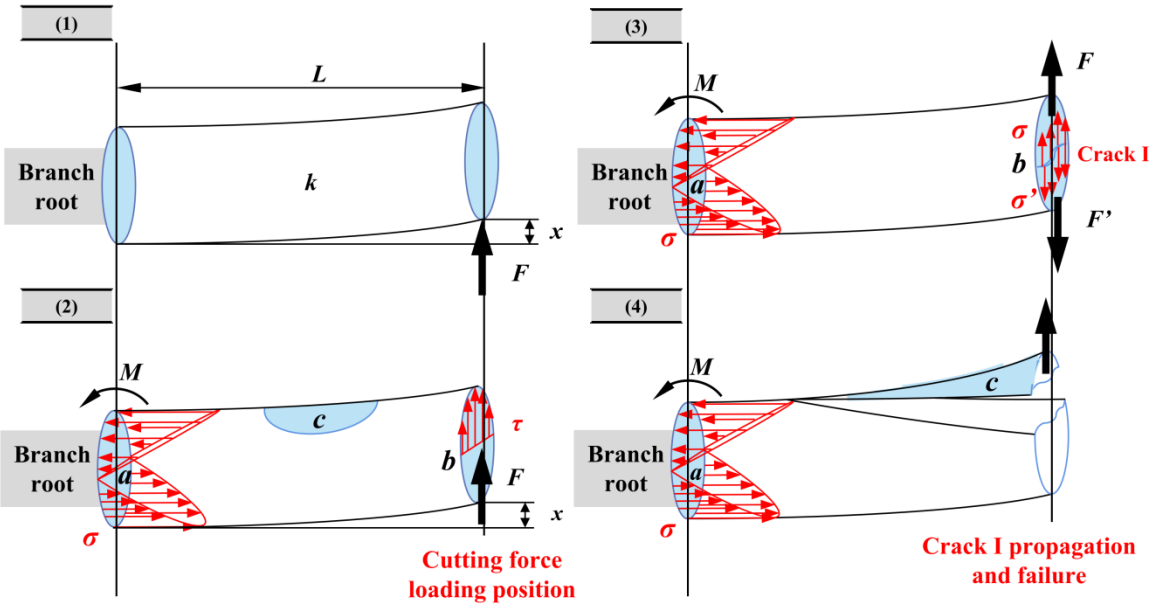

Fig. 3. Impact cutting mechanism analysis

At the macro level, the pruner should operate with a higher cutting force *F* to meet the operational requirements. However, the field results show that an increase in cutting force *F* is indeed conducive to improving pruning efficiency and quality, but there is no absolute correlation between cutting force *F* and branch failure mode. Therefore, an analysis of branch failure is needed.

When the cutter is in contact with the branch, the branch is subjected to a force along the direction of the cutting speed at the contact point of the branch and cutter. Under the action of the cutting force *F*, the root of the branch generates a bending moment *M*. At the root position, the diameter of the branch is the neutral axis, and the neutral axis is subjected to compressive stress on the upper side and tensile stress on the lower side, with a magnitude of σ. At the position of the contact point, the interior of the branch is subjected to a shear stress τ along the direction of the cutting speed, as shown in Fig. 3-(2). The maximum normal stress occurs at the root. At this point, according to the maximum tensile stress theory, when $\sigma > [\sigma]$, the root of the branch is damaged and broken, and the failure mode is branch impact failure. The stress σ applied to the root can be calculated by the following equations,

$$M_{max} = FL \quad (9)$$

$$W = \frac{\pi D^3}{32} \quad (10)$$

$$\boldsymbol{\sigma = \frac{M_{max}}{W}} \quad (11)$$

where $\boldsymbol{M}$ is the bending moment applied to the branch root (N*m), $\boldsymbol{W}$ is the section bending coefficient (m^3), and $\boldsymbol{L}$ is cutter-trunk clearance (m). There are also bending shear stresses in the root of the branch. However, based on pruning experience, normal stress is the main factor contributing to root failure. The analysis here ignores the factor of bending shear stress in the root.

If the cutter contacts the branch without root impact failure, as the contact process evolves, when $\boldsymbol{\tau} > [\boldsymbol{\tau}]$, then according to the maximum principal shear stress theory, the branch is destroyed by shear stress along the direction of the cutting speed, and the cutter cuts into the interior of the branch. The maximum shear stress occurs on the neutral axis of the section. That is, the branch undergoes cutting failure. At this time the shear stress $\boldsymbol{\tau}$ can be calculated by the following equations,

$$\boldsymbol{\tau_y = \frac{F_y S_z}{I_z b}} \quad (12)$$

$$\boldsymbol{S_z = \int_A y dA} \quad (13)$$

$$\boldsymbol{a = D \sin \beta} \quad (14)$$

$$\boldsymbol{I_z = \frac{1}{4}\pi b a^3 = \frac{1}{32}\pi b (D \sin \beta)^3} \quad (15)$$

$$\boldsymbol{\tau_y = \frac{32F \int_A y dA}{\pi b (D \sin \beta)^3}} \quad (16)$$

where $\boldsymbol{\tau}_y$ is shear stress applied to the branch (Pa), S_z is static moment (m^3), I_z is moment of inertia (m^4), D is the branch diameter (m), a is the length of the long axis of the ellipse (m), $\boldsymbol{\beta}$ is the cutter wedge angle (°), and b is the length of the short axis of an ellipse (m), as shown in Fig. 4.

From Eq. 16, when the branching angle increases, the shear stress decreases, making the branch failure process faster. From Eqs. 11 and 16, the increase of cutting force F will accelerate the process of branch failure and improve the cutting efficiency and cutting quality, but it will not have a decisive effect on the form of branch failure.

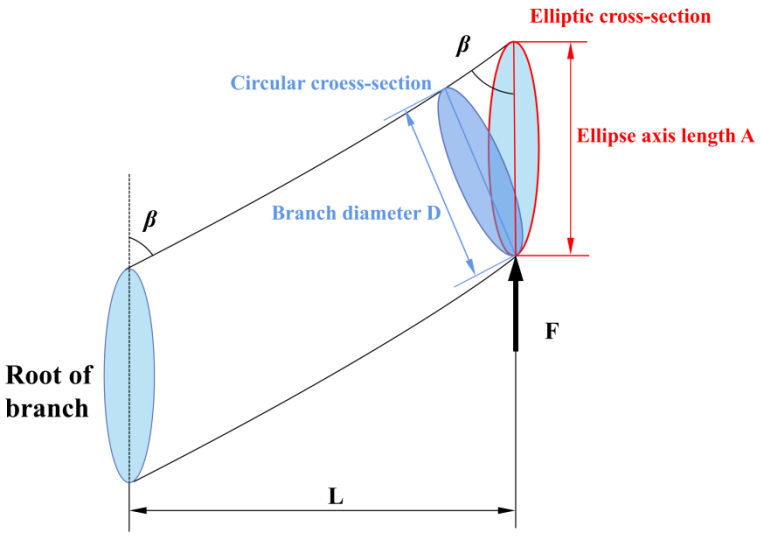

Fig. 4. Cutting speed direction cross-section analysis

Based on the hydraulic motor providing climbing power to the pruner, it can be determined that the cutter has enough power to cut into the branch until the branch fails. Under the impact load of the cutter, when the branch reaches the yield limit under the action of stress and fails, it will produce internal cracks. Under the influence of continuous stress loading, the crack will grow in the manner of unstable propagation. As the cutting process gradually proceeds, the stress concentration area inside the branch will be gradually concentrated in area **c** from areas **a**, and **b**, as shown in Fig. 3-(3). In the process of the branch cutting, cracks are gradually generated inside the branch. At this time, according to the knowledge of fracture mechanics, the force F loaded on the branch by the cutter produces a stress $\boldsymbol{\sigma}$ in the direction of cutting speed inside the branch, and there exists a reaction force F' inside the branch, which produces a stress $\boldsymbol{\sigma'}$ opposite to the direction of velocity inside the branch, as shown in Fig. 3c. Under the action of the two stresses, the branch produces a type I crack. In fracture mechanics, the stress intensity factor is generally used to describe the process of physical crack destabilization and expansion. The stress intensity factor K_I is,

$$\boldsymbol{K}_{\boldsymbol{I}} = \boldsymbol{\sigma f}\sqrt{\boldsymbol{\pi l}} \tag{17}$$

where $\boldsymbol{K_I}$ is the stress intensity factor ($\mathrm{MPa}\sqrt{\mathrm{m}}$), $\boldsymbol{f}$ is the geometric correction factor coefficient, and $\boldsymbol{l}$ is the crack size (m). When the cutting process enters the second half of the process, the stress $\boldsymbol{\sigma}$ and crack size gradually and gradually increase, and the stress intensity factor $\boldsymbol{K}$ gradually increases. According to the $\boldsymbol{K}$ criterion:

$$\boldsymbol{K_I = K_{IC}} \tag{18}$$

The criterion was proposed by G. R. Irwin, and $\boldsymbol{K_{IC}}$ is the critical stress strength factor of the material, which is related to the parameters of experiment temperature, material plate thickness, and deformation rate (Irwin 1958; Yarema 1996). The $\boldsymbol{K}$ criterion describes the critical conditions for the occurrence of extension behavior of the cracks inside the elastomer. Expansion of cracks occurs when the material reaches the critical condition of destabilized expansion. As shown in Fig. 3-(4), at this point the crack inside the branch gradually expands until the branch fails completely. At this point, there will be a laceration failure that occurs only in Region $\boldsymbol{c}$. In laceration failure, a large number of cracks are generated in the region of the branch loaded with stress and gradually expand to cause the branch to break completely.

The quality of branch pruning affects the health of trees as well as the quality of the wood. Too long pruning stubble will lead to unhealthy phenomena such as tree tumors and knots; poor pruning cross-section will lead to insect pests (Degent *et al.* 2022; Lyu *et al*. 2023). Incontrovertibly, it contributes to advancing the quality of the intervention on *Populus tomentosa* by analyzing impact cutting mechanism. According to the above analysis, it is known that the factors affecting the branch failure mode are: branch diameter $\boldsymbol{D}$, branch angle $\boldsymbol{\beta}$, cutting clearance $\boldsymbol{L}$, and branch material properties. This will guide the subsequent pruning operations and set the appropriate cutting parameters to meet the pruning needs.

It would be ideal to have an equation that, while not specific to any one species of tree, characterizes the failure pattern of branches (Davim 2013; Aguilera and Davim 2014). The factors affecting the branch failure mode include branch diameter d, branch angle $\boldsymbol{\beta}$, and cutting clearance $\boldsymbol{L}$. Summarizing an equation describing the branch failure mode is the expectation of this study, as shown in Eq. 19,

$$\boldsymbol{H \sim f(\gamma, D, \beta, L)} \quad (19)$$

where $\boldsymbol{\gamma}$ is the surface coefficient of the branch to describe the defect of the branch surface. It takes values in the range [0, 1]. The more severe the surface defect, the smaller $\boldsymbol{\gamma}$. When the surface is free of defects, $\boldsymbol{\gamma}$ = 1. The number of experiment samples required to obtain an empirical formula consisting of multiple factors is extremely large and the period required is extremely long. Equation 19 was simplified to reduce the number of experiment samples.

As shown in Fig. 4, branch diameter $\boldsymbol{D}$ and branch angle $\boldsymbol{\beta}$ are both natural growth factors of the branch. The cross-section of the branch in the direction of cutting speed is an ellipse, and the length of the long and short axes of the ellipse are:

$$\boldsymbol{A = 2a = \frac{D}{2 \sin \beta}} \quad (20)$$

$$\boldsymbol{A = 2b = \frac{D}{2}} \quad (21)$$

As shown in Eq. 20, the branch diameter $\boldsymbol{D}$ and the branch angle $\boldsymbol{\beta}$ are contained in the long axis of the ellipse $\boldsymbol{A}$. Therefore, the long axis A can be used instead of the above two parameters. The equation describing branch failure can be simplified as follows:

$$\boldsymbol{H \sim f(\gamma, A, L)} \quad (22)$$

In Eq. 22, according to the results of simulation analysis: the larger the long axis $\boldsymbol{A}$ is, or the smaller the cutting clearance $\boldsymbol{L}$ is, the branch failure mode tends to be cutting failure, *i.e.*:

$$\boldsymbol{H \propto A} \quad (23)$$

$$\boldsymbol{H \propto \frac{1}{L}} \quad (24)$$

Therefore, the branch failure equation is as follows.

$$\boldsymbol{H = \gamma \frac{A}{L}} \quad (25)$$

The branch failure eigenvalue is called $\boldsymbol{H}$, which is used to describe the branch failure state, and $\boldsymbol{H} > 0$. Obviously, the larger the eigenvalue $\boldsymbol{H}$ is, the closer the branch failure mode is to a cutting failure, and the smaller the eigenvalue $\boldsymbol{H}$ is, the closer the branch failure mode is to a root fracture or laceration failure. There is only eigenvalue $\boldsymbol{H}$ in the experimental parameters. It could reduce the experiment's complexity while ensuring accuracy.

Experimental Arrangements

Definition of experimental parameters

Table 1. Experiment Index and Factors

Experiment Index	Failure Patterns		
Level	Impact failure	Laceration failure	Cutting failure
	1	2	3
Factors	Branch diameter (mm)	Branch angle (°)	Cutting clearance (mm)
Level	10-20	50-60	5-15

According to the theoretical analysis, branch diameter ***D***, branch angle ***β***, and cutting clearance ***L*** are considered to be the main factors affecting the failure mode. Therefore, these three factors were selected as experiment factors. The factors and levels are shown in Table 1.

Experiment program and methods

In this paper, the experiment material, *Populus tomentosa* branches, was obtained in February 2023 from Baodi Plantation Forest Farm (39°46′33″N, 117°14′50″E), Tianjin, China. *Populus tomentosa* is a deciduous tree, and winter is a suitable season for pruning. After defoliation in winter, the water content of aspen branches is low and the branches are easy to prune (Maurin and Rochers 2013). To guarantee the branches were fresh, all samples were stored in sealed bags at room temperature at 25 ℃ after collection, and all experiments were completed within one week of branch collection.

The physical properties of the branches were tested using a universal testing machine (M4050, Wragle Instruments LTD, Shenzhen, China). The experiment system is shown in Fig. 5.

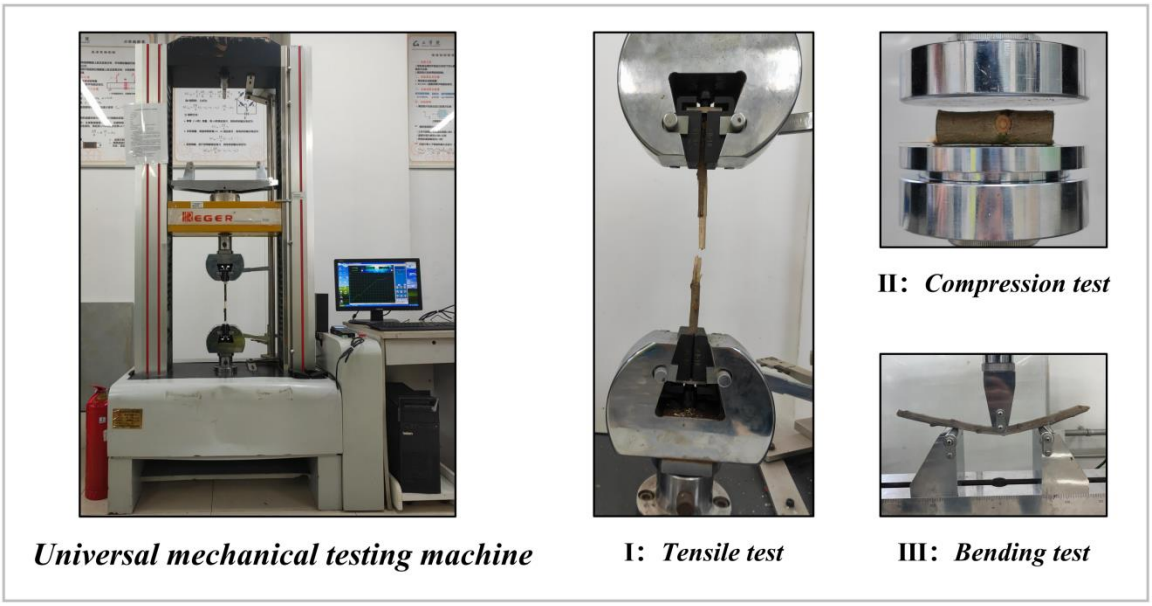

Fig. 5. Experiment system

The verification experiment site was located in the forest farm of Baodi District, Tianjin, China. The target tree was a 5- to 6-year-old *Populus tomentosa*, and the equipment was an impact pruner (Ban *et al*. 2022). After pruning, the branches were collected to measure the diameter and branch angle, and the characteristic eigenvalues were calculated. A digital camera was used to capture the failure section of the branch, and the failure mode was recorded and compared with the simulation results to analyze the correctness of the branch's theoretical model. The failure mode of branches under about 100 sets of data with different eigenvalues was collected. The influence of the eigenvalues on the branch failure mode was determined by fitting the sample data. The sample data were plotted as ***H-Y*** images and analyzed statistically.

The data without defects on the surface of the branches from the verification experiment was selected to be recorded, that is, γ=1. In order to avoid a large number of

overlapping data points in the image, small adjustments were made to the size of the data point levels for the same failure mode without affecting the results.

Simulation Modeling

In this paper, the finite element method-based explicit dynamics simulation is used to investigate the failure mode of branches under impact cutting. The research in this section mainly includes the idealization of the branch material model of the branch, the geometric model reconstruction, and the construction of the finite element model. The flow of the study is shown in Fig. 6.

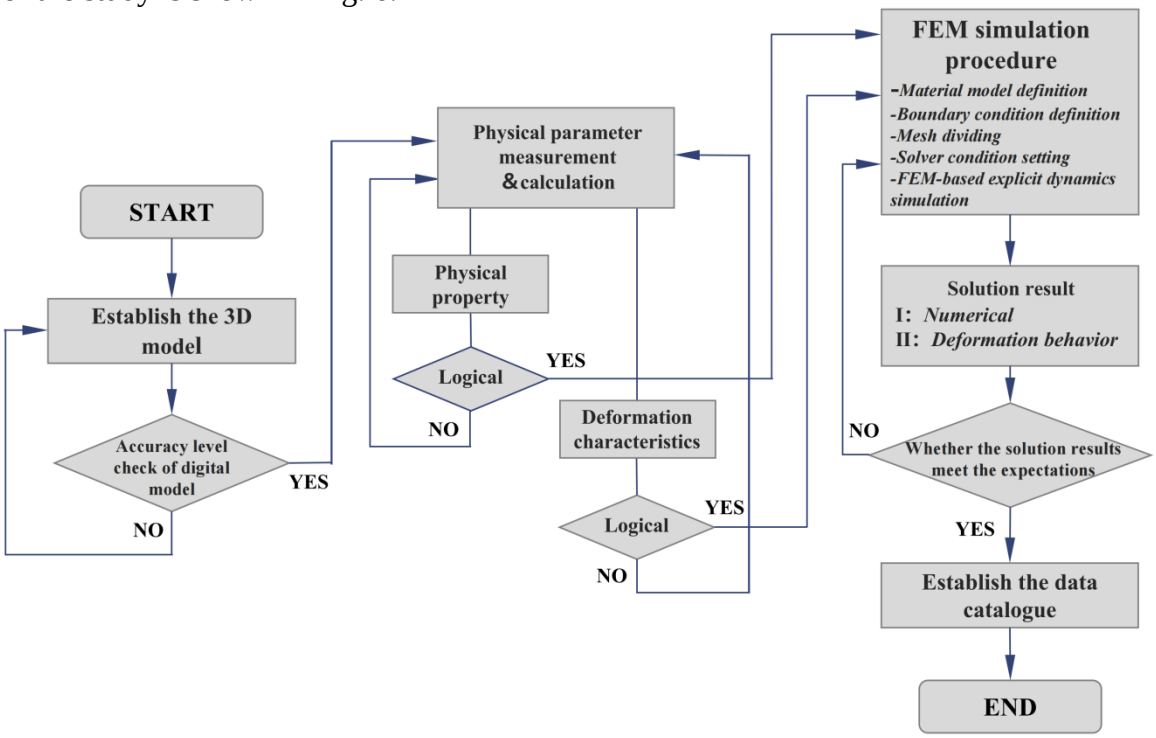

Fig. 6. Steps of explicit dynamics simulation procedure

Geometric model reconstruction

In agroforestry research, although the focus of the research is different, it is usually necessary to characterize the geometry of the research target (Yousefi *et al*. 2016). The impact pruner task is shown in Fig. 1. Appropriate simplification of the geometric model can effectively reduce the solution time. In this paper, the research focuses on the process of cutter-branch interaction, which means the trunk and pruner parts can be simplified appropriately. According to the prior analysis, the main stress locations are the section along the cutting speed direction and the root of the branch. The trunk section is hardly affected. All cutters are made of manganese steel, which is a much stronger material than the branch. The historical pruning experience also illustrated the fact that the cutter almost had no damage. The rest of the pruner structure was also almost unaffected. Therefore, the pruner will be kept only in the cutter part and the mass of the pruner will be equated to the cutter by increasing the cutter density.

The branch and cutter 3D models were drawn using Solid Works (SolidWorks, Waltham, MA) software in preparation for the finite element solution.

Material model idealization procedure

Appropriate assumptions could be made to obtain an approximate solution under realistic conditions according to the objectives, during building the ideal model of the material (Celik 2017b). When the branch is assumed to be an elastomer at the moment of initial contact between the cutter and the branch, the cutting force F increases with increasing branch deformation. The branch itself exhibits anisotropy, nonlinearity, and elastoplasticity, unlike conventional engineering materials such as metals and plastics. However, the growth direction of the branching fibers is axially ordered, which also implies that the branches are homogeneous in the radial direction. The focus of this paper is on the failure mode of the branch in the cutting speed direction. Therefore, it can be assumed that the mechanical properties of branches are isotropic and homogeneous in the cutting speed direction. For failure along the cutting speed direction, when the plastic deformation exceeds the material threshold, the branch undergoes plastic deformation and fails. The criterion for branch fracture failure is evaluated as the maximum equivalent plastic strain.

In finite element analysis, isotropic hardened plastic material models are generally used for large strain becoming case studies. In this paper, the constitutive model of the branch is defined as a linear isotropic hardened plastic material model. Table 2 displays the parameters that the finite element model employed, which are obtained and calibrated by experiments. Table 2 also lists the relevant parameters of the cutter. The cutter density is calculated after equivalent pruning machine mass.

Table 2. Material Properties

Properties of Branch	
Parameters	Value
Density (kg*m^3)	0.386
Young's modulus E (GPa)	1.6
Shear modulus G (GPa)	0.62
Bulk modulus K (GPa)	1.3
Poisson's ratio μ	0.3
Plastic strain ε	0.056
Yield limit σ (MPa)	4.75
Static friction coefficient μ_1	0.531
Sliding friction coefficient μ_2	0.467
Properties of Cutter	
Density (kg*m^3)	128250
Young's modulus E (GPa)	200
Shear modulus G (GPa)	76.92
Bulk modulus K (GPa)	167
Poisson's ratio μ	0.3

Simulation program

A finite element method-based explicit dynamics simulation method was used to investigate the branch failure mode under impact cutting. The explicit dynamics module in ANSYS Workbench was used to simulate the branch pruning process. In the analysis setup, the simulator is set to solve the model to a final time of 0.02 s. The branch model used in the simulation was defined as a completely homogeneous material. The boundary conditions were defined as having frictional contact with a coefficient of kinetic friction of 0.531 and a coefficient of static friction of 0.467. The friction coefficient is obtained by test measurement. The connection type was defined as geometry interaction. The contact

type was modified to erosion control to make the branch fracture more visible. The interaction between the tool and the branch is defined by the velocity *v* in the boundary conditions, and the ***v*** = 4 m/s. In the simulation program, the acceleration of gravity is set to 9.8 $m*s^{-2}$. Parameters such as mass density, velocity, and gravity acceleration are introduced to simulate the inertial effect during impact cutting.

Choosing the appropriate mesh size is a critical step in finite element analysis. Mesh density not only affects the accuracy of the solution results but it also affects the computer solution time. Larger element sizes save time but reduce accuracy. A smaller element size will improve the accuracy of the solution, but at the same time it will increase the solution time. Therefore, the results of equivalent stresses at branch failure were studied to evaluate the mesh sensitivity for different sizes with the same settings defined.

RESULTS AND DISCUSSION

Results of the mesh sensitivity study for different branch diameters are shown in Fig. 7.

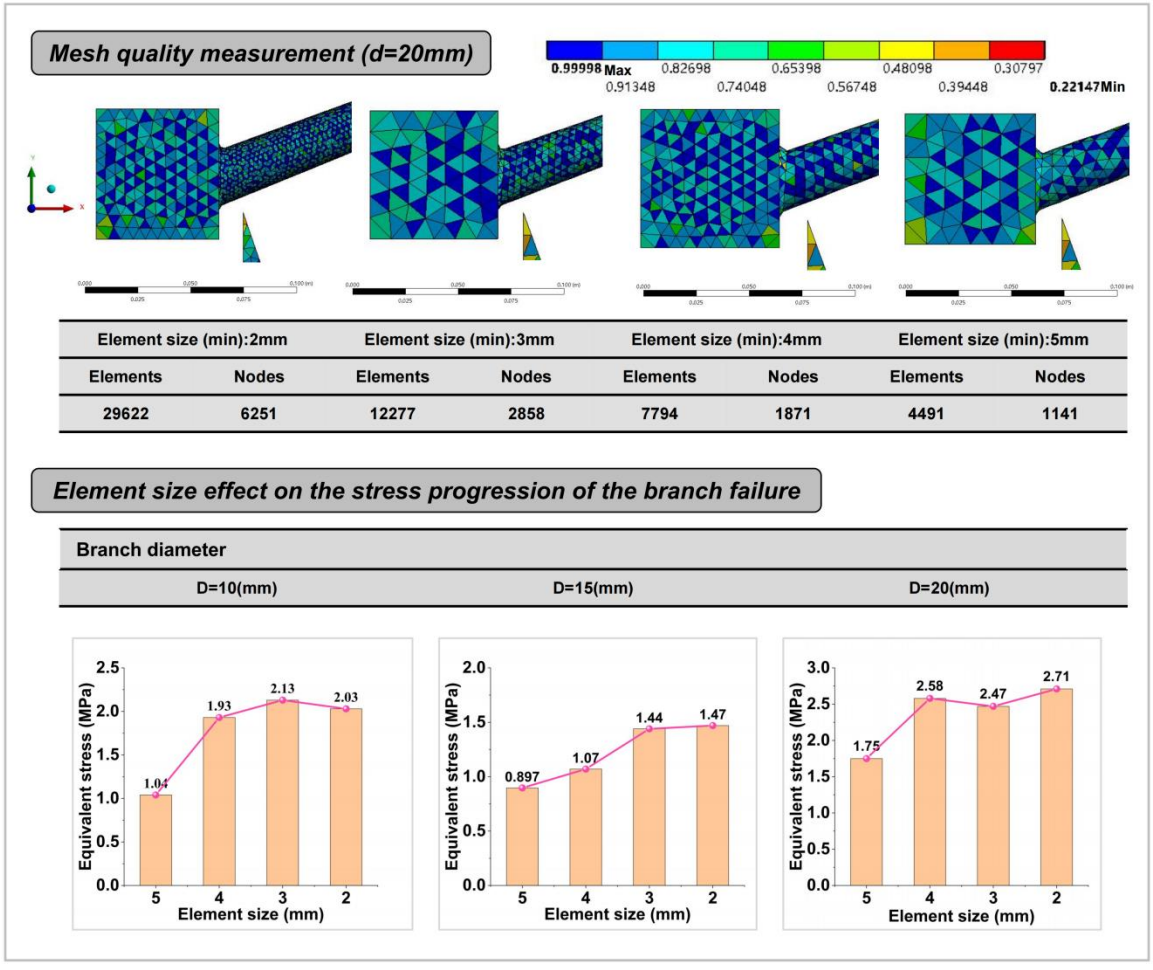

Fig. 7. Mesh sensitivity analysis and mesh structure details

The visualization of meshing for branch diameter D = 20 mm and the effect of all mesh sizes on the equivalent stress at failure for different branch diameters are demonstrated. The mesh sensitivity study shows that under the requirement of combining solution accuracy and solution time, it is more appropriate to select a mesh size of 4 mm for the samples with branch diameters D = 20 mm and D = 15 mm, and a mesh size of 3 mm for the branch diameter D = 10 mm branches. In the solution results, the equivalent stress and energy activities of branch, shear stress on the root, normal stress along the cutting speed direction are recorded in the branch failure process in each case.

After completing the pre-processing steps of the finite element simulator, the designed case was solved. The solution results can clearly describe the stress change process during the branch failure. As shown in Fig. 8, the stress cloud inside the branch under different failure modes, demonstrates the change of the stress magnitude and the change of the stress distribution area inside the branch as the cutting process proceeds. The stress-time curves in Fig. 8 include the normal stress of the branch root, the shear stress of cutting position, and the equivalent stress of the cutting process. Figure 9 demonstrates the variation of stress distribution region during branch failure. Table 3 demonstrates the values of all simulation results with failure mode. The last column shows the comparison of simulation results with experiment results.

Influence of Each Factor on the Failure Mode

Figure 8 shows the contribution of each factor in the branch failure process and the stress variation curve. The branch failure mode for branch diameter $\boldsymbol{D}$ = 10 mm is impact failure on the branch root; the branch failure mode for branch diameter $\boldsymbol{D}$ = 15 mm is cutting failure; and the branch failure mode for branch diameter 20 mm is the coupling of cutting failure and laceration failure.

The larger the branch diameter, the more the branch failure mode shows cutting failure mode, but the failure of large-diameter branches will be accompanied by the characteristics of laceration failure. When the branch angle is 50°, the failure mode is impact failure, but there are cases in which small-diameter branches deform elastically but do not fail in the solution results; when the branch angle is 60°, the failure mode is the coupling of cutting failure and laceration failure, and the tearing damage is more serious; when the branch angle is 70°, the failure mode is the coupling of cutting failure and laceration failure, and the laceration failure is mainly concentrated in the c-region. When the cutting clearance is 5 mm, the failure mode is strictly cutting failure; when the cutting clearance is 10 mm, the failure mode is laceration failure; when the cutting clearance is 15 mm, the failure mode is the impact failure on the root.

Comprehensive analysis, the main factors affecting the branch failure mode are branch diameter and cutting clearance. Changes in branch diameter and cutting clearance will affect the magnitude of normal stress at the root of the branch during cutting and the magnitude of shear stress in the direction of cutting speed, which will change the final failure mode of the branch.

As shown in Fig. 4, the branch angle affects the major axis length of the ellipse, which changes the magnitude of shear stresses and thus indirectly affects the branch failure mode. Therefore, the effect of branch angle on a branch failure mode is either superimposed or coupled.

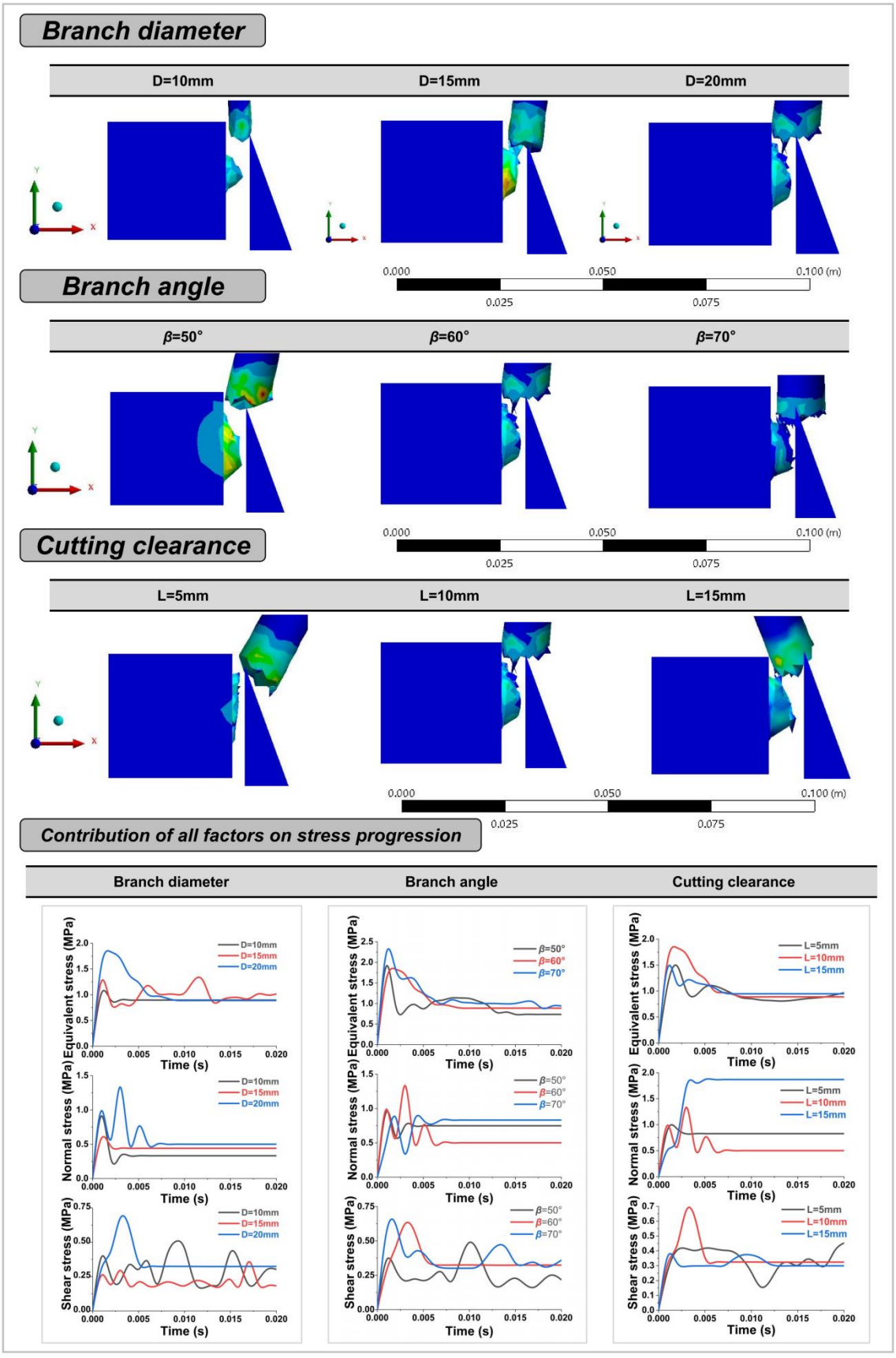

Fig. 8. Branch failure visuals and stress progression visuals

Table 3. Simulation Results

Branch diameter (mm)	Branch angle (°)	Cutting clearance (mm)	Failure pattern	Equivalent stress (max) (MPa)	Normal stress (max) (MPa)	Shear stress (max) (MPa)	Internal energy (max) (J)	Comparison
10	50	5	3	1.1521	1.1467	0.4621	0.4733	Y
		10	2	1.1270	1.0612	0.5411	0.8960	N
		15	2	1.8160	0.5550	0.3040	0.7670	Y
	60	5	3	1.2359	1.1496	0.4664	0.4783	Y
		10	2	1.2720	0.9139	0.3960	0.8488	N
		15	*	1.3907	0.5571	0.5179	0.1462	Y
	70	5	3	1.8778	1.7293	0.4830	0.4743	Y
		10	3	2.5003	1.6358	0.2975	0.4374	Y
		15	2	1.9128	1.9024	0.5233	0.7661	Y
15	50	5	3	1.6017	1.3401	0.5717	0.1560	Y
		10	3	1.7271	0.5661	0.4354	0.3479	N
		15	2	2.0971	0.6313	0.5356	0.9315	Y
	60	5	3	1.9298	1.8051	0.6531	0.2633	Y
		10	1	1.9288	0.7165	0.3718	0.2140	Y
		15	2	2.2843	1.0356	0.3702	0.8431	Y
	70	5	3	1.6200	1.5578	0.2795	0.3452	Y
		10	2	2.5053	1.1131	0.4016	0.9287	Y
		15	2	2.3518	1.5555	0.6834	0.8946	Y
20	50	5	3	1.5582	1.5100	0.4893	0.4135	Y
		10	1	1.9164	0.9551	0.4745	0.4705	Y
		15	1	1.9342	0.6059	0.4946	0.4207	Y
	60	5	3	1.4831	0.9186	0.4178	0.5212	Y
		10	1	1.4283	1.3873	0.4422	0.3856	Y
		15	1	1.4600	1.0869	0.3644	0.4595	Y
	70	5	3	1.8452	1.7166	0.4069	0.4512	Y
		10	3	2.5815	1.1408	0.7689	0.4079	Y
		15	3	2.5977	0.9821	0.3942	0.4158	Y
* The branch deforms but does not fail.								

Stress Behavior of Branch Failure

Inside the branch where cutting failure occurs, the stress maximum tends to be concentrated at the tip loading location, and the branch reaches its yield limit and fails under the stresses loaded by the cutter. The maximum stress tends to be concentrated in the c-region. When the cutter initially contacts the branch, the maximum stress is still concentrated in the tip region, and the b-region reaches the yield limit under stress and is destroyed, at which time cracks occur inside the branch. When the c-region stress increases with the cutting process, the branch c-region cracks under stress expansion speeds up, and eventually tear failure occurs in the c-region.

Inside the branch where root impact failure occurs, the stress maximum is mainly concentrated at the branch root location. The stress maximum occurs first at the tip of the cutter when the cutter contacts the branch. As the cutter makes deeper contact with the branch, the value of stress at the root increases instantaneously and exceeds the yield limit of the branch, so that the branch fails at the root location. All the processes occur at the instant of cutter impacts the branch, and the whole process is generally over within 0.01 s, and therefore is called impact failure. In particular, it should be added that in this case, the severed portion of the branch acquires an initial velocity that is much greater than the

remaining two failure modes, and the direction of the velocity is at an acute angle to the direction of the pruner speed. The whole process is similar to the elastic collision in rigid-body dynamics. As shown in Table 3 and Fig. 8, the shear and normal stresses change more drastically during branch failure. This suggests that the branch fails under their coupled effects rather than a single factor. The branch damaged area of the laceration failure is so large that the internal energy is much greater than that of the cutting and impact failures.

From the stress time curve in Fig. 8, it can be seen that the magnitude of the normal stress at the root of the branch only shows a surge at the moment when the tip of the knife contacts the branch, and the whole is in a relatively stable state during the cutting process. The normal stress change image is basically consistent with the analysis described earlier. The change of shear stress shows an oscillating phenomenon with large amplitude, which reflects that the shear loading area shape is changing during the branch failure process, and on the other hand, the axial tearing caused by the expansion of internal cracks in the branch is also affecting the magnitude of shear stress. The magnitude of the equivalent stress on the branch during the cutting process shows a surge at the moment that the tip of the knife touches the branch, and the equivalent stress under different failure modes varies from one to another. In the case of root impact failure, the equivalent stress is more stable; in the case of cutting failure, the equivalent stress changes more frequently, but the peak of the equivalent stress is basically concentrated at the beginning of branch failure.

A summary of the energy activity is a significant indicator of the accuracy of the results of the simulation showing the dynamics. Among the energy activities, kinetic energy, internal energy, contact energy, plastic energy, and hourglass energy can be examined. Hourglass is an unphysical zero-energy deformation behavior in finite element analysis that does not strain the generating mesh cell (*e.g.*, hexahedral cell). The energy activity generated by it is known as hourglass energy (Wallmeier *et al*. 2015). In general, scholars recommend that the hourglass energy does not exceed 5% to 10% of the internal energy (Dewulf *et al*. 1999). Figure 9 shows a plot of the energy summary of the model and a demonstration of the deformation behavior in one of the solution results. The deformation results of the branch in all the solution results were basically consistent with the physical tests, and the hourglass energy was also lower than 5 to 10% of the internal energy value. Another way to test the results of a finite element solution is by observing whether the deformation behavior of the model matches the deformation behavior of the physical test. Combining the characteristics of the deformation behavior and the state of the energy activity during the branch failure, it can be judged that the solution results under this finite element method-based explicit dynamics model were accurate.

The simulation results indicate that stress change, rather than cutting force, provides a more precise and complete explanation of the branch failure process. An essential factor in the pruning process and the design of the pruning machine is the cutting force, which can be used to characterize the difficulty of removing branch material (Luo *et al*. 2016; Li *et al*. 2022). Nevertheless, neither the deformation behavior of the branch nor the fracture features of the failed piece of the branch can be described by the cutting force. Stress can reflect the microscopic removal features of fibers and describe the force interaction between interior tissues during branch deformation. Stress behavior-based models are better able to expound on the reasons for various failure scenarios and describe the branch damage process. Stress is an effective method that more precisely indicates how much tissue is removed during crop harvesting. This aligns with the findings of Li *et al*. (2015).

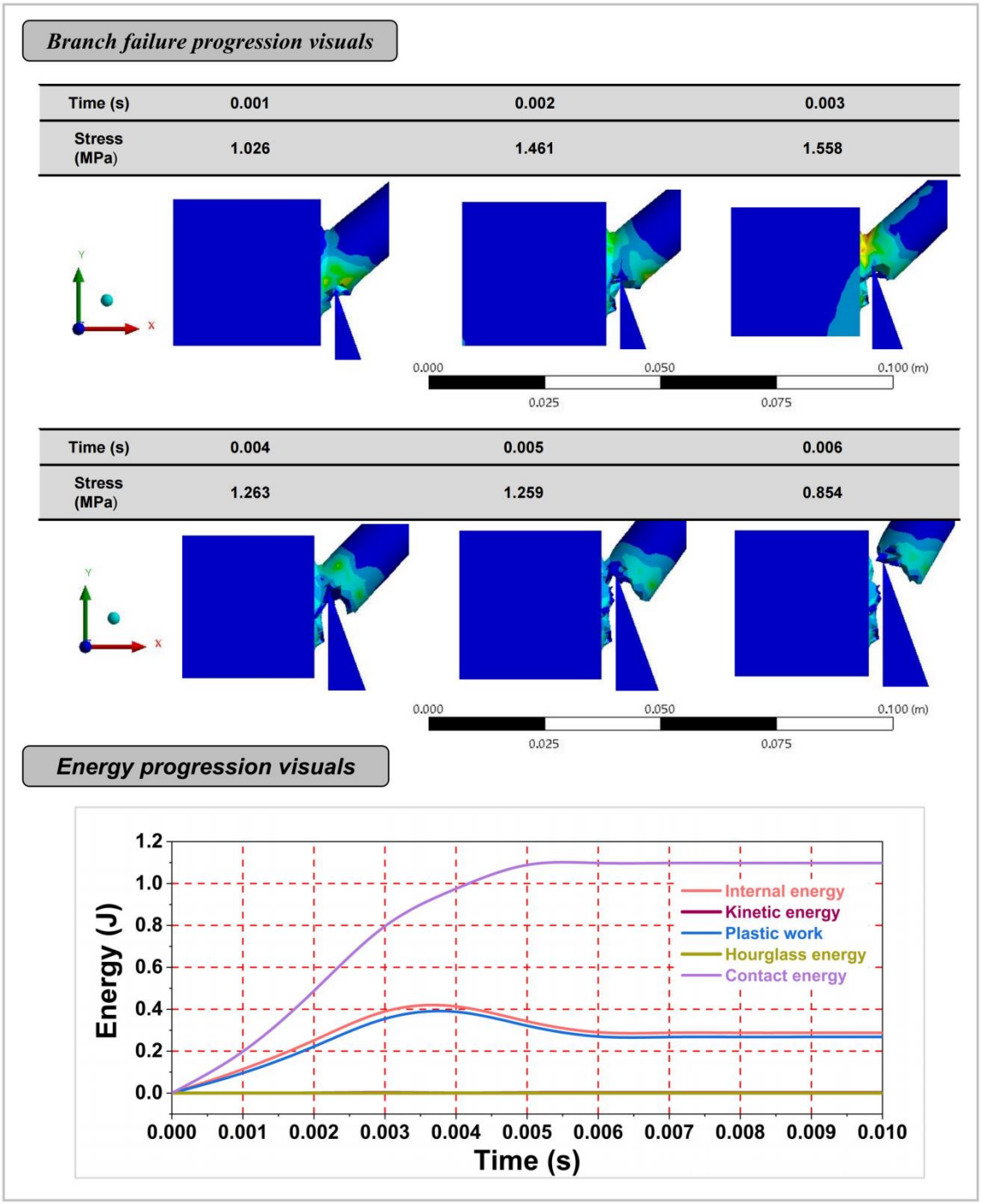

Fig. 9. Branch deformation behavior and energy activity in the progression of failure

The impact of internal cracks on section quality is explained by the branch failure model developed in this research. One important component affecting the branch failure characteristics is the crack's size, whose generation and extension are dominated by stress variations. The load's influence on the crack's extension will ultimately cause the branch to fail. This aligns with previous findings (Pichler *et al*. 2018; Brandstätter *et al*. 2023).

VERIFICATION EXPERIMENT

The last column of Table 3 shows the comparison of simulation results with experimental results. Y (meaning "yes") indicates that the simulation results were consistent with the experiment results, and N indicates that they were inconsistent. According to the experiment data, the consistency between the simulation results and the experiment results was between 88.9% and 92.6%. When branch diameter *D* was 20 mm, the simulation results were basically consistent with the experimental results. When branch diameter *D* was 15 mm, there was a small error between the simulation results and the experiment results. When branch diameter *D* was 10 mm, there were more errors between simulation and experiment results. In the experiment results, the sample with branch diameter *D* = 10 mm showed several elastic deformities without failure, which also appeared in the simulation results. The reason for this phenomenon may be that these samples were newly grown, and their tissue was relatively soft, so the physical properties were elastomeric, which is also consistent with the elastic hypothesis in the theoretical analysis. Therefore, the results of finite element simulation can be considered reasonable, combined with the experiment results. The experimental results also showed that the mechanism proposed in this paper can explain the failure process of branches more accurately.

The results of the interforest pruning experiment are shown in Fig. 10. The results showed that the cutting failure was the main failure mode of the branch with the increase of branch diameter and the quality of pruning. With the increase of cutting clearance, the quality of pruning became worse, and the failure mode of branches was only impact failure. The change of branching angle had less effect on failure mode than other factors, but the increase of branching angle was beneficial to improve pruning quality. The failure mode of branches with increased eigenvalue was mainly cutting failure. According to Eqs. 20 and 25, the increase of eigenvalue implies increasing values of branch diameter and the decrease of cutting clearance, which means the decrease of normal stress at the root of the branch. The reduction of normal stress causes cutting failure rather than impact failure. In the cantilever beam model, when the diameter of the branch increases, the yield limit of the cantilever beam increases, and the branch will not tear failure.

The sample data of branch failure equation verification experiment were plotted as ***H*-*Y*** images, as shown in Fig. 10. The experiment shows that, when the eigenvalue ***H*** was small, the branch failure mode presented the root impact failure mode. As the eigenvalue ***H*** was increased, the branch failure mode gradually transitioned from the root impact failure to the laceration failure, and the pruning quality decreased. As the eigenvalue ***H*** continued to increase, the branch failure mode gradually transitioned to the cutting failure. The experiment results were basically consistent with the simulation results.

However, it should be noted that the continuous increase of the eigenvalue does not guarantee that the branch failure mode is cutting failure in the absolute sense. As shown in Fig.10c, where the eigenvalue ***H*** was the largest, the branch failure mode was instead a laceration failure. In this region, the branch diameter is large (***d*** > 15 mm) and the cutting clearance is relatively small (***L*** < 10 mm). The reason for this situation may be that when the cutter cuts into the interior of the branch, the number of type I cracks generated is large (much larger than the small-diameter branch), and a large number of cracks are destabilized and expanded, leading the branch to produce a laceration failure mode. The variability of the branch structure leads to variability in the results of the same eigenvalues when repeated experiments are performed, as in the region of Fig. 10d. It is also important to

note that although the overall branch failure mode obeys the law characterized by the eigenvalue ***H***, there are still sample data in various regions that did not conform to the expected law. For example, there were also cases in regions a and b where the eigenvalues were small and cutting failure or laceration failure still occurred. At the same time this part of the branch in the pruning process, there was also the occurrence of elastic deformation behavior, but no failure. The deformation behavior of the branches during pruning is affected by their physiological conditions, showing great uncertainty. In general, the branch failure eigenvalues can accurately describe the branch failure mode.

In summary, the failure mode of *Populus tomentosa* branches under impact pruning can be described by the eigenvalue ***H***. The proposed branch failure eigenvalue *H* could be expected to predict the failure mode of the branch. The experimental results also support that the branch impact cutting mechanism proposed in this paper was more accurate, and it was able to elaborate the failure process of the internal tissues, especially the stress behavior, of the plant stems in the impact operation, with the *Populus tomentosa* branch as an example.

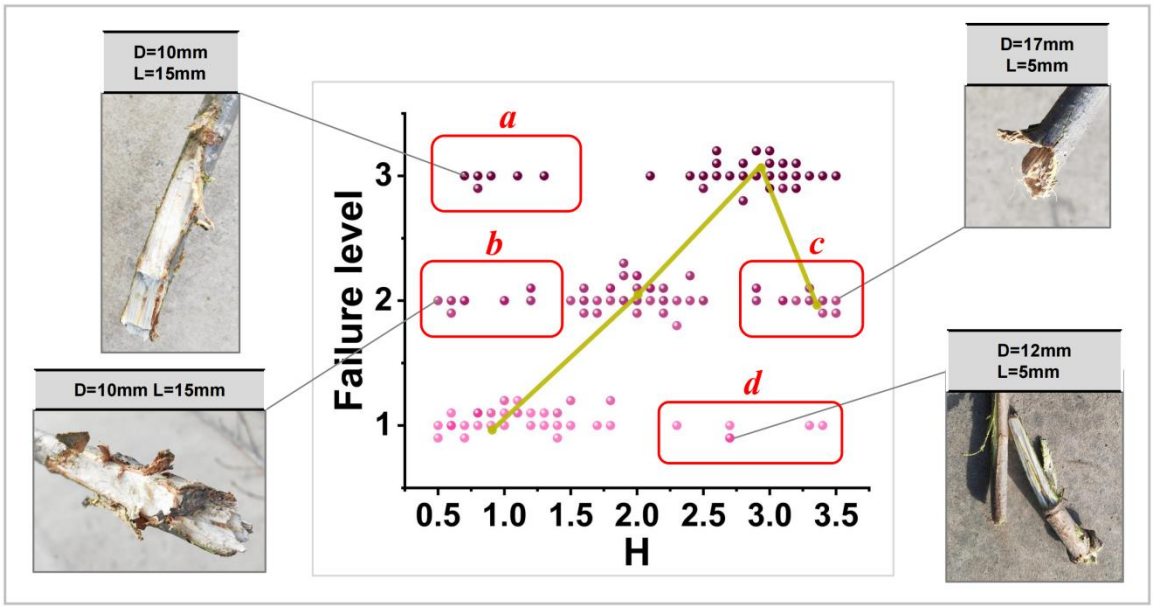

Fig. 10. Branch failure verification experiment

CONCLUSIONS

1. A branch failure model with branch diameter, cutting clearance, and branching angle as the key factors was established to describe the impact cutting failure process of branches. The cutting force generation, internal stress change, and crack propagation behavior during the process from elastic deformation to failure were analyzed in detail in the branch failure model under impact cutting. The branch failure state equation is proposed to describe the failure mode of the impact cutting branch, which can accurately describe the failure mode of the branch.
2. An explicit dynamic simulation method based on finite element analysis is proposed to study the impact cutting process. By studying the stress and deformation behavior of the branches in the simulation results, the effects of branch diameter, cutting clearance,

and branch angle on the failure mode of the branches were obtained. The results show that stress variation and crack propagation behavior of branches can accurately explain the dynamic process of impact failure of branches. The finite element explicit dynamic method is an effective tool to study the failure process of plant stems.

3. The research results revealed the failure mechanism of the impact cutting of branches and supplemented the lack of impact cutting theory. The introduction of the finite element explicit dynamic method provides a new way to study the large load and deformation problems in forestry field. The research results can provide theoretical support for the research and development of plant stalk cutting equipment, especially in the aspects of performance optimization and structure optimization.

ACKNOWLEDGMENTS

This research was supported by the National Natural Science Foundation of China (Grant No. 32071679).

REFERENCES CITED

Aguilera, A., and Davim, J. P. (2014). *Research Developments in Wood Engineering and Technology*, IGI Global. DOI: 10.4018/978-1-4666-4554-7

ANSYS Documentation. (2016). *Release Notes: Explicit Dynamics Analysis. Release 17.1*. Canonsburg, PA: ANSYS, Inc.

Ban, Y. C., Lyu, K., Ba, S. H., Wen, J., Kang, F., and Li, W. B. (2022). "Monkeybot: A climbing and pruning robot for standing trees in fast-growing forests," *Actuators* 11(10), article 287. DOI: 10.3390/act11100287

Brandstätter, F., Autengruber, M., Lukacevic, M., and Füss, J. (2023). "Prediction of moisture-induced cracks in wooden cross sections using finite element simulations," *Wood Science and Technology* 57, 671-701. DOI: 10.1007/s00226-023-01469-3

Celik, H. K. (2017a). "Determination of bruise susceptibility of pears (Ankara variety) to impact load by means of FEM-based explicit dynamics simulation," *Postharvest Biology and Technology* 128, 83-97. DOI: 10.1016/j.postharvbio.2017.01.015

Celik, K. K. (2017b). "Explicit dynamics simulation of Pecan fruit deformation under compressive loading—Part-2: Explicit dynamics simulation procedure," *Journal of Food Process Engineering* 6, article 40. DOI: 10.1111/jfpe.12582

Davim, J. P. (2011). *Finite Element Method in Manufacturing Processes*, Wiley. ISBN: 978-1-848-21282-4.

Davim, J. P. (2013). *Wood Machining*, Wiley. ISBN: 978-1-118-60267-6.

Degnet, M. B, Werf, E., Ingram, V., and Wesseler, J. (2022). "Community perceptions: A comparative analysis of community participation in forest management: FSC-certified and non-certified plantations in Mozambique," *Forest Policy and Economics* 143, article 102815. DOI: 10.1016/j.forpol.2022.102815

Dewulf, W., Jancsók, P., Nicolai, B., Roeck, G. D., and Briassoulis, D. (1999). "Determining the firmness of a pear using finite element modal analysis," *Journal of Agricultural Engineering Research* 74(3), 217-244. DOI: 10.1006/jaer.1999.0451

Food and Agricultural Organization (FAO). (2016a). "Trees, forests and land use in drylands: The first global assessment," Rome, Italy.

Food and Agricultural Organization (FAO). (2016b). "Poplars and other fast-growing trees-renewable resources for future green economies," Synthesis of Country Progress Reports, International Poplar Commission. (25)13-16, Berlin, Germany. http://www.fao.org/3/a-mt504e.pdf

Fu, J. Y., Zou., S. Y., Coleman, M., Li, X. M., Hu, W., Wang, A. Y., Zhang, P., Zeng, Z. Z., Ding, C. J., Xi, B. Y., and Di, N. (2022). "Is it necessary to apply chemical weed control in short-rotation poplar plantations on deep soil sites?" *Industrial Crops & Products* 184, article 115025. DOI: 10.1016/j.indcrop.2022.115025

Gowda, R. V. P., Murthy, A. N. N., and Muniraju, E. (2011). "Development of design methodology for mechanized harvesting and pruning of shrubs," *Indian Journal of Science and Technology* 4, 101-106. DOI: 10.17485/ijst/2011/v4i2.2

Guan, X. D., Li, T. Y., and Zhou, F. J. (2023). "Determination of bruise susceptibility of fresh corn to impact load by means of finite element method simulation," *Postharvest Biol. Technol.* 198, article 112227. DOI: 10.1016/j.postharvbio.2022.112227

Hartley, M. J. (2002). "Rationale and methods for conserving biodiversity in plantation forests," *Forest Ecol. Manag.*155, 81-95. DOI: 10.1016/S0378-1127(01)00549-7

Irwin, G. R. (1958). "Fracture," in: *Handbuch der Physic* 6, 551-590.

Jordan, E. (2019). "Machine for debranching living trees," US Patent 10,470,382, B2.

Li, B., Zhang, Z. K., Li, W. G., and Peng, X. R. (2015). "A numerical simulation on multi-spot pressure tensioning process of circular saw blade," *J. Wood Sci*. 61, 578-585. DOI: 10.1007/s10086-015-1508-5

Li, C. J., Zhang, H. S., Wang, Q. C., and Chen, Z. J. (2022). "Influencing factors of cutting force for apple tree branch pruning," *Agriculture* 12, article 312. DOI: 10.3390/agriculture12020312

Luo, Y. Q., Ren, Y. H., Zhou, Z. X., Huang, X. M., and Song, T. J. (2016). "Prediction of single-tooth sawing force based on tooth profile parameters," *International Journal of Advanced Manufacturing Technology* 86, 641-650. DOI: 10.1007/s00170-015-8201-0

Lyu, J. H., Qu, H. Y., and Chen, M. (2023). "Influence of wood knots of Chinese weeping cypress on selected physical properties," *Forests* 14(6), article 1148. DOI: 10.3390/f14061148

Mathanker, S. K., Grift, T. E., and Hansen A. C. (2016). "Effect of blade oblique angle and cutting speed on cutting energy for energy cane stems," *Biosystems Engineering* 133, 64-70. DOI: 10.1016/j.biosystemseng.2015.03.003

Maurin, V., and Rochers, V. D. (2013). "Physiological and growth responses to pruning season and intensity of hybrid poplar," *Forest Ecology and Management* 304, 399-406. DOI: 10.1016/j.foreco.2013.05.039

Meng, Y. M., Wei, J. D., Wei, J., Chen, H., and Cui, Y. S. (2019). "An ANSYS/LS-DYNA simulation and experimental study of circular saw blade cutting system of mulberry cutting machine," *Computers and Electronics in Agriculture* 157, 38-48. DOI: 10.1016/j.compag.2018.12.034

Ni, Y. L., Jin, C. Q., Chen, M., Yuan, W. S., Qian, Z. J., Yang, T. X., and Cai, Z. Y. (2021). "Computational model and adjustment system of header height of soybean harvesters based on soil-machine system," *Computers and Electronics in Agriculture* 183, article 105907. DOI: 10.1016/j.compag.2020.105907

Niu, Z. J., Xu, Z., Deng, J. T., Zhang, J., Pan, S. J., and Mu, H. T. (2022). "Optimal vibration parameters for olive harvesting from finite element analysis and vibration

tests," *Biosystems Engineering* 215, 228-238. DOI: 10.1016/j.biosystemseng.2022.01.002

Pichler, P., Leitner, M., Grun, F., and Guster, C. (2018). "Evaluation of wood material models for the numerical assessment of cutting forces in chipping processes," *Wood Sci Technol* 52, 281-294. DOI: 10.1007/s00226-017-0962-1

Shah, D. U., Reynolds, T. P. S., and Ramage, M. H. (2017). "The strength of plants: theory and experimental methods to measure the mechanical properties of stems," *Journal of Experimental Botany* 68(16), 4497-4516. DOI: 10.1093/jxb/erx245

Song, S. Y., Zhou, H. P., Xu, L. Y., Jia, Z. C., and Hu, G. M. (2022). "Cutting mechanical properties of sisal leaves under rotary impact cutting," *Industrial Crops and Products* 182, article 114856. DOI: 10.1016/j.indcrop.2022.114856

Tom Leblicq, T., Vanmaercke, S., Ramon, H., and Saeys, W. (2015). "Mechanical analysis of the bending behaviour of plant stems," *Biosystems Engineering* 129, 87-89. DOI: 10.1016/j.biosystemseng.2014.09.016

Wang, C. S., Hein, S., Zhao, Z. G., Guo, J. J., and Zeng, J. (2016). "Branch occlusion and discoloration of *Betula alnoides* under artificial and natural pruning," *Forest Ecology and Management* 375, 200-210. DOI:10.1016/j.foreco.2016.05.027

Wallmeier, M., Linvill, E., Hauptmann, M., Majschak, J. P., and Östlund, S. (2015). "Explicit FEM analysis of the deep drawing of paperboard," *Mechanics of Materials* 89, 202-215. DOI: 10.1016/j.mechmat.2015.06.014

Xi, B. Y., and Clothier, B. (2021). "Irrigation management in poplar (*Populus* spp.) plantations: A review," *Forest Ecology and Management* 494, article 119330. DOI: 10.1016/j.foreco.2021.119330

Yang, W., Zhao, W. J., Liu, Y. D., Chen, Y. Q., and Yang, J. (2021). "Simulation of forces acting on the cutter blade surfaces and root system of sugarcane using FEM and SPH coupled method," *Computers and Electronics in Agriculture* 180, article 105893. DOI: 10.1016/j.compag.2020.105893

Yarema, S. Y. (1996). "On the contribution of G. R. Irwin to fracture mechanics," *History of Fracture Mechanics* 31, 617-623. DOI: 10.1007/BF00558797

Yousefi, S., Farsi, H., and Kheiralipour, K. (2016). "Drop test of pear fruit: Experimental measurement and finite element modelling," *Biosystems Engineering* 147, 17-25. DOI: 10.1016/j.biosystemseng.2016.03.004

Zeng, Z. Z., Wang, D. S., Yang, L., Wu, J., Ziegler, A. D., Liu, M. F., Ciais, P., Searchinger, T. D., Yang, Z. L., Chen, D. L., Chen, A. P., Li, Z. X., Piao, S. L., Taylor, D., Pan, M., Peng, L. Q., Lin, P. R., Gower, D., Feng, Y., Zheng, C. M., Guan, K. Y., Lian, X., Wang, T., Wang, L., Jeong, S. J., Wei, Z. W., Sheffield. J., Caylor. K., and Wood, E. F. (2021). "Deforestation-induced warming over tropical mountain regions regulated by elevation," *Nature Geoscience* 14, 23-29. DOI: 10.1038/s41561-020-00666-0

Zhou, J., Xu, L. Y., Zhang, A. Q., and Hang, X. C. (2022). "Finite element explicit dynamics simulation of motion and shedding of jujube fruits under forced vibration," *Computers and Electronics in Agriculture* 198, article 107009. DOI: 10.1016/j.compag.2022.107009

Article submitted: February 26, 2024; Peer review completed: April 6, 2024; Revised version received and accepted: April 12, 2024; Published: April 18, 2024.
DOI: 10.15376/biores.19.2.3614-3636